

Machine Learning methods for Automatic Vessel Segmentation

in Fundus Images



Kushal Khandelwal

Birla Institute of Technology and Science,Pilani

This thesis is submitted in partial fulfillment of the requirements of the
course BITS C422T

May 2015

Acknowledgements

First, I would like to thank my thesis advisor Professor Fred Hamprecht, whose constant guidance and support has helped me to learn a lot while working towards the thesis. I would like to thank him for providing me this opportunity to write my thesis in his group. I would also like to express my sincere gratitude to Dr. Ferran Diego, who has always been an excellent mentor and a guide. His constant feedback during the entire duration of thesis has helped me complete my thesis in Heidelberg. I would also like to thank my co-mentor Dr. Melih Kandemir for his valuable feedback.

I also want to thank all the current and former member of the Multidimensional Image Processing group for those invaluable discussions and suggestions and for making the time at Heidelberg Collaboratory for Image Processing much more fun. I would also like to thank my on campus supervisor in India Dr. Sukanta Mondal, for helping me throughout the duration of thesis at various stages.

I would like to thank my parents and my sister, for being with me all the time and be the constant pillar of support in my life. Thank you, for being patient and keeping me motivated during the entire duration of my work.

Last but not the least, I would like to thank the coordinators of Erasmus Mundus mobility with Asia (EMMA) , for providing the financial support and making this exchange possible.

Table of contents

List of figures	vii
List of tables	ix
1 Introduction	1
1.1 Motivation	1
1.2 Outline of thesis	3
2 Background and Literature Review	5
2.1 Machine Learning	5
2.2 Clustering	6
2.2.1 K-Means Clustering	7
2.3 Spare Coding and Dictionary Learning	9
2.4 Literature Review	10
3 Framework	13
3.1 Vessel segmentation Framework	13
3.1.1 Learning Architecture	15
3.2 Cluster Learning	15
3.2.1 Learning	16
3.2.2 Prediction	17
3.2.3 Algorithm	18
3.3 Dictionary Learning	18
3.3.1 Learning	19
3.3.2 Prediction	21
3.4 Datasets	21
3.4.1 DRIVE	21
3.4.2 STARE	22
3.4.3 ARIA	22

3.4.4	CHASEDB1	23
4	Experimental Evaluation and Results	25
4.1	Vessel Segmentation Assessment	26
4.2	Generalization of the model	31
5	Conclusion and Future Work	37
	References	39

List of figures

1.1	A diseased fundus image	2
1.2	Architecture for the problem of automated segmentation of retinal vessels.	3
2.1	K-Means Visualization	8
3.1	Fundus Image and its segmentation	14
3.2	Training architecture for our learning model.	16
3.3	Local structures learned using clustering and their segmentation maps	18
3.4	Dictionary of image atoms and segmentations	20
4.1	Red, Green, Blue channels of a fundus image	26
4.2	Image segmentation using varying patch sizes	27
4.3	ROC curve with varying patch size	28
4.4	Image segmentation using varying the number of clusters	29
4.5	ROC and PRC curve for Cluster Learning based model	30
4.6	ROC curve comparing the best and worse case on DRIVE set	30
4.7	Results on DRIVE dataset	32
4.8	ROC curve on a train test split of STARE dataset	33
4.9	Best case on DRIVE test dataset using cluster learning	33
4.10	Worst case on DRIVE test dataset using cluster learning	34
4.11	Cross training comparison for STARE dataset	35

List of tables

3.1	Summary of Datasets	23
4.1	STARE performance for different training sets	31

Chapter 1

Introduction

1.1 Motivation

With the advancement in medical imaging, computer aided diagnostic(CAD) systems have become a vital part of today's medical diagnosis [7]. CAD systems have become a part of routine clinical work and are being used extensively for disease diagnosis. A myriad of different medical imaging systems, like X-Ray, Magnetic Resonance Imaging (MRI), Computed Tomography Scans etc, are used for diagnosis. The output of such systems are multidimensional digital images, interpretation of which require sophisticated digital image processing methods. Automated medical diagnosis systems can aid in easy and faster interpretation of these images.

Digital fundus imaging in ophthalmology is a vital component in diagnosis of various pathologies like Diabetic Retinopathy(DR), glaucoma and age related macular degeneration(AMD). Retinal vessel segmentation forms an important part of diagnosis of such pathologies. Changes in the retinal vasculature is precursor to many diseases such as diabetes, hypertension and stroke. Morphological properties such as diameter, length, branching angle, of the retinal vessel forms an important component in diagnosis and evaluation of ophthalmologic diseases such as glaucoma and hypertension. For example, vessel diameter measurement can be an aid in diagnosis of hypertension [3].

Vessel segmentation is a challenging and a tedious task which may take a couple of hours when performed manually. Problems like low contrast between vessel and background, noise in the image and variability in the width, brightness and shape alongwith the presence of exudates, lesions, hemorrhage spots and other pathological effects make the task much more

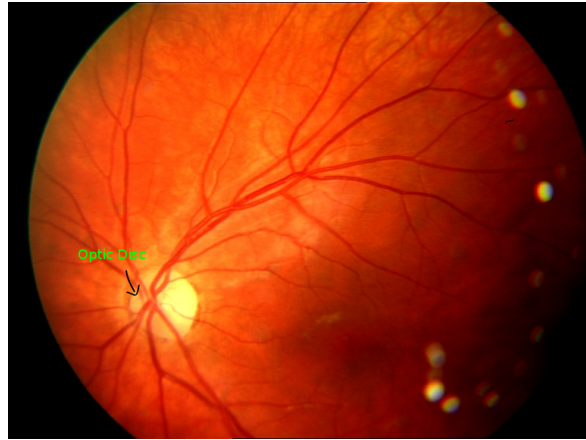


Fig. 1.1 A diseased fundus image

difficult. Figure 1.1 shows a fundus image of a diseased eye.

Developing an automated retinal vessel segmentation is a first step towards developing a full fledged CAD system for diagnosis of ophthalmology pathologies. There have been a lot of work in literature on automatic retinal segmentation, including based on matched filtering [1, 18, 49], tracking methods [5, 31], morphological methods [23, 48], and learning based methods [14, 35, 41]. One of the simpler approach to segmentation utilizes adaptive thresholding to segment out the blood vessels [20]. Another simple approach is to use edge detection techniques like canny edge detector for vessel segmentation [4].

Some of the more sophisticated models use learning based algorithms which learn on a set of given image segmentations. Many of these models, learn local features at a pixel location and train a pixel classifier. Nguyen et al. [34] present the limitations in some of the existing methods and presents a multi-scale line detection based method for blood vessel segmentation. Issues, like poor segmentation at bifurcation and crossover regions, merging of close vessels and poor segmentation of small vessels limit the application of vasculature based medical diagnosis. For example, merging of two nearby vessels can lead to vessel being considered as one wide vessel, thereby affecting the width measurements of the vessel. These limitations may contribute to inaccuracies in vascular network analysis and subsequently in characterization of the underlying disease.

Supervised learning methods, in general are limited by the amount of training data. Also most of them are restricted to the type of training data and do not generalize on the task at hand. In this thesis, we propose two supervised learning models for accurate vessel

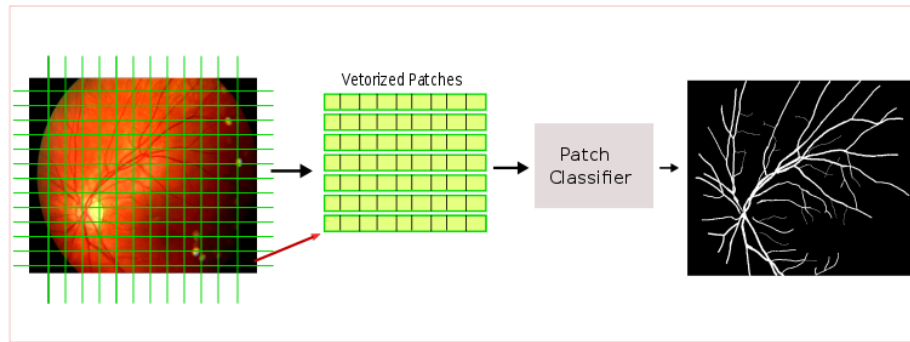


Fig. 1.2 Architecture for the problem of automated segmentation of retinal vessels.

segmentation. Our method is a patch-based framework that learns the local structure of the vessel at patch level. An illustrative architecture of our framework is shown in figure 1.2, exploits the presence of common structures in a typical vascular tree. Unlike most of the supervised learning methods which make a prediction at pixel level, classifying each pixel as vessel or background, our model predicts the local structure around each pixel at patch level, giving a structured output for each patch. We show that our model generalizes well over different training data and is somewhat robust to changing imaging parameters like field of view and resolution.

1.2 Outline of thesis

The thesis is organized as follow,

- Chapter 2 provides some background knowledge on machine learning and used algorithms. It is followed by a brief overview on existing work on blood vessel segmentation. Finally, we explain in detail some of the methods by which our work is inspired.
- Chapter 3 starts by defining our patch-based framework for vessel segmentation. We then explain our models based on cluster learning and dictionary learning.
- Chapter 4 presents the evaluations and experimental results of our methods applied to three datasets. We present the effect of different setting on the performance. We also compare our evaluations with some of the work in the literature.
- Chapter 5, finally gives our concluding remarks and sets the tone for future work.

Chapter 2

Background and Literature Review

In this chapter we present a brief introduction on the basic background knowledge for this thesis. We start by giving an overview on basics of machine learning. We then discuss in detail the clustering and dictionary learning algorithms. A discussion on sparse coding for dictionary learning is done in this sections. Later we talk about some of the relevant work from literature. In the last section we briefly describe some of the latest state-of-art methods which inspired our work.

2.1 Machine Learning

Machine learning is the study dealing with the process of extracting and learning, useful and relevant information from data. Given some data, X , a machine learning algorithm learns a function $f(X)$ which maps the input X to an output variable y . The learned model then can be used to make predictions on previously unseen data X' . A machine learning algorithm learns the parameters of an adaptive model from a training set, typically by optimizing a function. The learned model is then used to make predictions on previously unseen new data. Broadly, machine learning methods can be divided into two subfields, supervised learning and unsupervised learning. In a supervised setting the target labels or values are known for the training set and we focus on predicting the target value for previously unseen data. In an unsupervised setting no such target information is present for the training data and the focus is to learn structure and compact descriptions from the data.

In a supervised setting, given a set of labeled data points known as the training data:

$$T = \{(x_1, y_1), \dots, (x_n, y_n)\}$$

, where $x_i \in X$ and $y_i \in Y$, we find a function f , which maps any point in the domain of X to its corresponding label in Y . If Y is a set of discrete values then it is known as a classification problem and if Y is in a continuous range then it is a problem of regression.

In an unsupervised setting, the task is to find group relations between instances of the unlabeled training dataset with a subsequent aim of categorizing or clustering the data. The algorithm finds the previous unknown structure in the data.

The data point x_i is typically represented as a vector comprising of feature values and is known as a feature vector. For example, given a dataset $X = \{x_1, x_2, \dots, x_m\}$ where x_i is an image patch of size $\sqrt{n} \times \sqrt{n}$, each patch can be represented as a vector of length n formed by concatenating the gray scale values. The entire dataset then can be represented as a matrix:

$$X = \begin{pmatrix} x_{1,1} & x_{1,2} & \cdots & x_{1,n} \\ x_{2,1} & x_{2,2} & \cdots & x_{2,n} \\ \vdots & \vdots & \ddots & \vdots \\ x_{m,1} & x_{m,2} & \cdots & x_{m,n} \end{pmatrix}$$

Here each row of the matrix denotes individual data points and $x_{i,j}$ is the gray scale intensities of patch x_i at pixel location j .

2.2 Clustering

A cluster is collection of data points grouped together on basis of some common properties. The data objects or points within a cluster are similar to each other, whereas the points outside the cluster are dissimilar.

The process of partitioning these data points into smaller groups (called as clusters) with an aim to minimize the intra cluster variance and maximize the inter cluster variance, is known as clustering. The grouping of data points is based on the similarity or dissimilarity of the objects as described by their properties or features.

Similarity or dissimilarity between two objects can be very subjective and hence various metrics are used to describe them quantitatively with distance measure being the most common. The distance measure is used to calculate the distance between two objects and then be used to create a distance matrix called as similarity/dissimilarity matrix. The most

commonly used distance metric is the Euclidean Distance.

The Euclidean distance D between two points $p = \{x_1, x_2, \dots, x_n\}$ and $q = \{y_1, y_2, \dots, y_n\}$ can be defined as:

$$\begin{aligned} dist(p, q) &= \sqrt{(x_1 - y_1)^2 + (x_2 - y_2)^2 + \dots + (x_n - y_n)^2} \\ &= \sqrt{\sum_{i=1}^n (p_i - q_i)^2} \\ &= \|\mathbf{p} - \mathbf{q}\| \end{aligned} \quad (2.1)$$

As the data labels are unknown, cluster analysis is known as an unsupervised method of data partitioning. This is in contrast to classification where the data can be partitioned on the basis of their class labels. Thus, clustering segments the data based on properties of the objects within the dataset and finds previously unknown grouping within the data.

2.2.1 K-Means Clustering

In this section we look into the K-Means clustering algorithm (MacQueen et al. [27]). We assume that the number of clusters 'K' is given and we use it to initiate our clustering algorithm. The idea is to partition the dataset into 'k' clusters and assign 'k' centroids, one for each cluster

Given a dataset $D = [x_1, x_2, \dots, x_n]$ consisting of n objects, where each object is a feature vector of length 'm'. The clustering algorithm partitions the dataset into 'K' clusters C_1, C_2, \dots, C_k such that $C_i \subset D$ and $C_i \cap C_j = \emptyset$ and with an aim to have a low intra cluster variance and a high inter cluster variance. This means that the points within the same cluster must be highly similar and dissimilar to the points belonging to other clusters.

The partitioning is performed in an iterative manner and follows what is known as Lloyd's algorithm [21]. We initialize the 'k' centroid by some initialization methods such as k-means++ or random initialization. The cluster quality depends on a good initialization. We start by assigning each point in the dataset to the nearest nearest centroid and we get 'k' clusters. We then calculate the mean points of the new clusters and assign them as the new centroids. The process then continues till a stopping criterion is reached. The partitioning is made with an aim to minimize the objective function which is the within cluster sum of squared error.

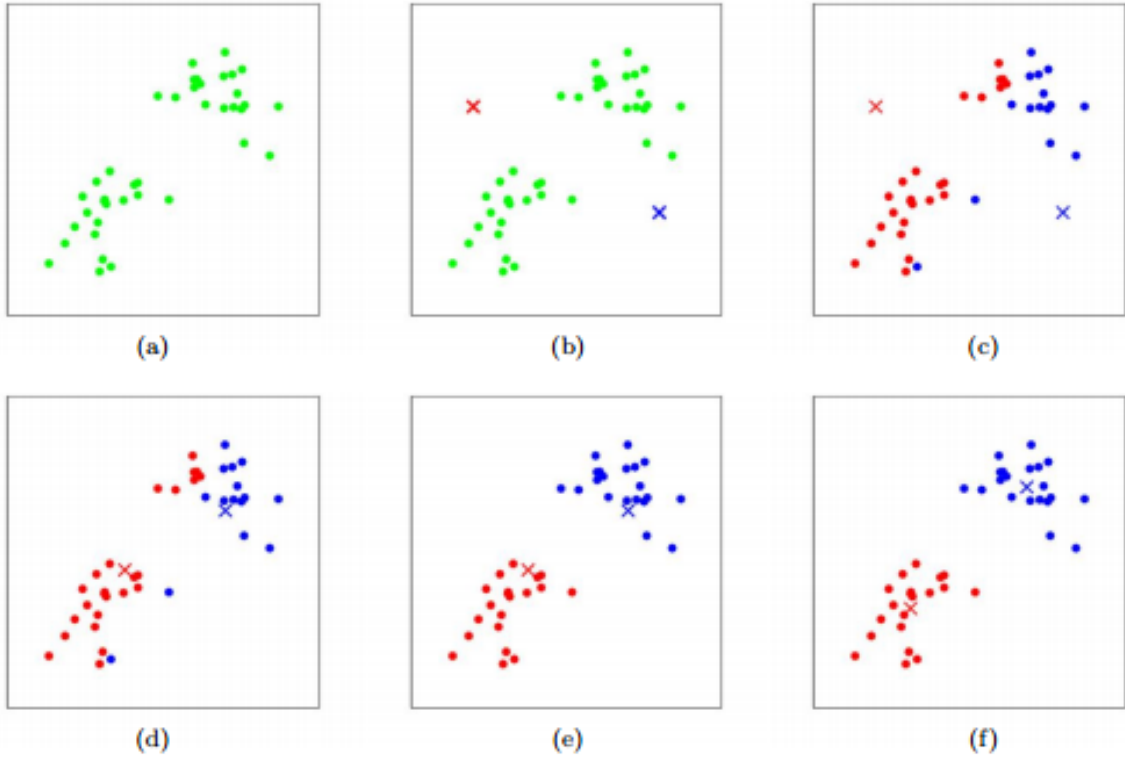


Fig. 2.1 K-means algorithm. The training examples are shown as dots, with cluster centroids shown as crosses. (a) Original dataset. (b) Random initial cluster centroids. (c-f) Illustrates the running two iterations of k-means algorithm. In each iteration, we assign each training example to the closest cluster centroid (points belonging to common cluster are shown in same color); then the cluster centroid is updated as the mean of new points assigned to the cluster. (Images courtesy of Michael Jordan. Retrieved from : <http://stanford.edu/~cpiech/cs221/handouts/kmeans.html>)

Each of the clusters C_i consists of p points and is represented by its centroid c_i . The distance between point p and the cluster center c_i is defined as $dist(p, c_i)$. If the data points are in m dimensions, then the distance can be computed as in Eq 2.1. We can then write our objective function J as :

$$J = \sum_{j=1}^K \sum_{i=1}^p \| \mathbf{x}_i^{(j)} - \mathbf{c}_j \|^2 \quad (2.2)$$

K-means clustering is the simplest unsupervised learning algorithm and can be applied to many different problems. An example of K-Means clustering on a toy dataset with 2 clusters is shown in Figure 2.1

2.3 Spare Coding and Dictionary Learning

The process of learning a finite set of basis elements, called atoms, from a given training set of signals $X = [x_1, x_2, \dots, x_n]$, such that each signal in X can be approximately reconstructed by a linear combination of atoms is called Dictionary Learning. These finite sets of atoms, D , is the learned dictionary. Normally we want to find a sparse decomposition of signals in D i.e, we aim to create a dictionary of sparse elements. This kind of decomposition is different from PCA where the basis elements have to be orthogonal to each other and these dictionaries are in general overcomplete.

By overcomplete here we mean that if any element from the dictionary is removed, we can still approximately reconstruct the signal from the atoms. Also the number of atoms in dictionary is of a greater dimension than the data. Lewicki and Sejnowski [25] describes the process of learning overcomplete set of representations. Some recent work [30] has shown that sparsity captures high-order correlation in data and it captures higher order statistics in data.

Huang and Aviyente [19] talks about how to represent a given signal as a sparse decomposition of a dictionary D . In a sparse coding task, our goal is to represent a signal $x \in \mathbb{R}^m$, as a linear combination of an overcomplete dictionary $D = [d_1, d_2, \dots, d_k] \in \mathbb{R}^{n \times k}$. Here 'k' is the no of atoms $d_k \in \mathbb{R}^n$. To ensure that the dictionary is overcomplete, we have $k > n$. The task is to find a representation in form a sparse code vector α of $k \times 1$, such that:

$$\alpha = \min_{\alpha'} \|\alpha\|_0, \quad s.t \quad x = D\alpha, \quad (2.3)$$

where $\|\alpha\|_0$ is l0 norm, which represents the number of non-zero components in α .

It has been found that this problem is hard to solve and thus we replace l0-norm with l1-norm, so then as others (Lee et al. [24], Donoho [9]), the problem is reformulated to find α by minimizing the objective function J:

$$J(\alpha; \lambda_1) = \min_{\alpha \in \mathbb{R}^k} \|x - D\alpha\|_2^2 + \lambda_1 \|\alpha\|_1 \quad (2.4)$$

where the parameter λ_1 is the regularization parameter which ensures a trade off in sparsity and reconstruction error. It also ensures that the sparse codes are not very large.

To further ensure that the dictionary values D , do not become arbitrarily large, Mairal et al. [28] constrains the columns of D to have an l_2 -norm less than or equal to one.

For our purpose we use the Online dictionary learning implementation of Mairal et al. [28]. This is a very efficient method and scales well for millions of training examples. Sparse coding is done using the orthogonal matching pursuit (OMP) method [36, 45] implemented in the SPAMS library provided by Mairal et al. [29]

2.4 Literature Review

In this chapter we aim to present a general overview of vessel segmentation methods. We particularly focus on approaches based on machine learning methods both supervised and unsupervised techniques. There has been a considerable work in the domain of automatic retinal vessel segmentation. Fraz et al. [12] provide a detailed review of retinal vessel segmentation methods. We briefly outline some of the methods before we move on to explain the most recent supervised learning based algorithms.

The earliest work on retinal segmentations are based on tracking methods to trace the blood vessels [6, 44]. In these methods the vessel is traced out from some starting seed points according to some relevant criterion. Recently, Vlachos and Dermatas [47] proposed a methods based on multi scale line tracking. They approach the problem by tracking the retinal vessel at multi scales and combining the individual image maps at different scales. Farnell et al. [10] employ multi scale line operators at various orientations to enhance the blood vessels.

There has been a recent surge in utilizing supervised machine learning based methods for vessel segmentation. In such methods, generally, each image pixel is represented as a feature vector computed using local or global information. A classifier is then trained to label every pixel as vessel or background. Such classifiers rely on the training dataset, which is not available easily. Ricci and Perfetti [37] proposed a supervised classifier using line operators and using support vector classification. They obtain unsupervised pixel classification by thresholding the response of basic line detector. Additionally, they use orthogonal line detectors along with grey level of target pixel to construct feature vector for support vector machines based supervised classification. Staal et al. [42] proposed a ridge based vessel segmentation method used together with a supervised learning technique. Nguyen et al. [34] proposed a method utilizing gabor filter responses at multiple scales as features for pixel

classification. [16, 46] proposed neural network bases approach to vessel segmentation

We now look in detail some of the existing methods for retinal vessel segmentation.

Dollár and Zitnick [8] recently proposed a structured learning framework for predicting local edges utilizing random forests. Their work exploits the presence of local structure forms like straight lines or T-junctions in image patches to learn an accurate edge detector. They train random forests in structured output spaces. Local image labels are highly interdependent and utilizing the knowledge on such local structures tend to improve the the classifiers accuracy. The problem of edge detection is formulated in a way to predict local segmentation maps for input image patches. The structure labels are mapped to proxy discrete labels, in a way that similar structure labels are assigned to same discrete labels. Using this proxy mapping, existing random forest training approaches are used to learn structured random forests. Finally these forests are used to label each pixel to denote the presence or absence of edges.

Rigamonti and Lepetit [38] proposed a method to learn ad hoc features with learned filters. Many hand crafted features have been proposed to solve the problem of extracting linear structures like blood vessels, but are not always effective. In contrast, learned features are better at the task but are computationally expensive. The proposed algorithm complements handcrafted features with learned filters. Linear filters are computed from training images in a convolutional approach. The convolutional filters are constrained to be dissimilar. Further, feature maps are computed by convolving the learned filters with the images. Several such feature maps our computed both for handcrafted features like Optimally oriented flux (OOF) [22], Enhancement Filtering (EF) [11] and for learned filters. These features maps are then used to calculate descriptors at each image location. A random forest classifier is then trained to classify each image pixel as lying on a linear structure or background.

Ganin and Lempitsky [15] proposed a very elegant approach to natural edge detection or thin object segmentation. They employ a combination of convolutional neural networks with the nearest neighbor search. The problem is approached in a patch based framework, where the predictions are made patch by patch, and the the output of all the patches are combined to reconstruct the final output image. The approach is to pair a parametric model with a large number of parameters , with a non parametric mapping, to account for the underfitting. They observer that for the complex transforms like natural edge detection, neural networks show a strong underfitting and thereby a suboptimal performance. The proposed method works by first learning a convolutional neural net classifier CNN with some parameter θ . Then some

random patches with known output annotations are passed through the CNN classifier, to obtain an intermediate mapping of patches \mathcal{P} to the CNN output as $CNN(\mathcal{P})$. Since the annotations of these patches are known, a dictionary is created of the intermediate CNN output to known output annotations like $D = \{CNN(P) : A(P)\}$. Finally, at test time each patch is then passed through the CNN classifier to obtain the intermediate mapping, which is then search used a kNN classifier on the dictionary to obtain the ground truth annotation for each patch.

Chapter 3

Framework

In this chapter we present the basic framework of our vessel segmentation method. We start by setting up the various notations used throughout the chapter and give an overview about how the framework is applied. Next we discuss the two different models applied in the framework. This forms the core of this thesis and represents the major work done. At last we mention the various datasets utilized to test our models. In the next chapter we experimentally evaluate the models.

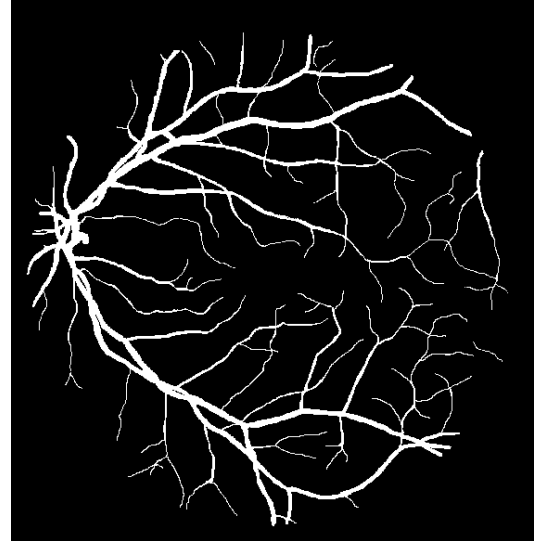
3.1 Vessel segmentation Framework

We start by defining the basic notations and methods. The input to our vessel segmentation framework is a training set composed of fundus images and their corresponding segmentation or label maps. The collection of fundus images is represented by $\bar{I} = (I^{(1)}, I^{(2)}, \dots, I^{(n)})$ and their corresponding ground truth segmentation maps as $\bar{S} = (S^{(1)}, S^{(2)}, \dots, S^{(n)})$. Each given image is of size $M \times N$. For simplicity, in the rest of the section we would refer an image as I and its segmentation map as S . We also assume that the image I is a single channel image.

We can represent an image as a collection of overlapping patches computed around every pixel take at center. A patch is of size $\sqrt{n} \times \sqrt{n}$ unless otherwise noted. We represent a patch centered at location (x, y) as $p_{x,y}$, and patches for I and S can be represented as $Ip_{x,y}$ and $Sp_{x,y}$ respectively. For simplicity we would refer the pixels of patch as p_i for $i = [1 \dots n]$, where ' i ' is the pixel location. A patch can also be represented as a vector, obtained by concatenating the image patch values.



(a) Fundus Image



(b) Segmented Vessels

Fig. 3.1 Fundus Image and its segmentation

We then represent our dataset with each image in terms of their patches as:

$$I = \begin{pmatrix} I^{(1)}p_1 & I^{(1)}p_2 & \dots & I^{(1)}p_n \\ I^{(2)}p_1 & I^{(2)}p_2 & \dots & I^{(2)}p_n \\ \vdots & \vdots & \ddots & \vdots \\ I^{(M)}p_1 & I^{(M)}p_2 & \dots & I^{(M)}p_n \\ \vdots & \vdots & \ddots & \vdots \\ I^{(N)}p_1 & I^{(N)}p_2 & \dots & I^{(N)}p_n \end{pmatrix}, S = \begin{pmatrix} S^{(1)}p_1 & S^{(1)}p_2 & \dots & S^{(1)}p_n \\ S^{(2)}p_1 & S^{(2)}p_2 & \dots & S^{(2)}p_n \\ \vdots & \vdots & \ddots & \vdots \\ S^{(M)}p_1 & S^{(M)}p_2 & \dots & S^{(M)}p_n \\ \vdots & \vdots & \ddots & \vdots \\ S^{(N)}p_1 & S^{(N)}p_2 & \dots & S^{(N)}p_n \end{pmatrix} \quad (3.1)$$

Fig 3.1 shows an example of fundus image on the left and the corresponding segmentation image on the right.

The aim of our thesis is to learn a function F which maps the image to its segmentation as, $F : I \rightarrow S$, i.e, we want to learn a function to segment the vessel in a given fundus image. Inspired by the work of [26, 32] we approach the problem of predicting segmentation maps in a patch based framework. In this patch level method, to predict the segmentation map for an image I , we decompose the image into overlapping patches and predict the segmentation maps for individual patches in a patch by patch fashion. The image and the segmentation map after decomposition can be represented as in Equation 3.1. Here ' I ' denotes the fundus

image and 'S' its segmentation map.

At the test time, we compute the patches for a given image and the mapping function F is then used to predict the segmentation map for all the test patches. Finally, the output segmentation patches are combined by averaging, resulting in an output segmented image. As the patches are computed in an overlapping way, to each pixel several segmentation patches are added during reconstruction phase. More precisely, each pixel is composed of N pixel values from N nearby patches.

3.1.1 Learning Architecture

The major part of our work is to learn an effective mapping function F , to map the fundus image to its segmentation map. In both of our models we learn local structure representations in form of a dictionary. This dictionary is composed of patches representing the edge structures, T-junctions, crossovers, parallel lines and other commonly occurring local patterns. To these patches is associated their ground truth segmentations. At prediction time, we then approximately decompose each patch as a linear combination of dictionary elements. To compute the final segmentation of the patch, each atom of the dictionary element in the linear combination is replaced by its segmentation.

An example of the learning model is shown in figure 3.2. Both of the models presented in the section, learn this dictionary for predicting the ground truth map. Before we delve into our models, we list the common preprocessing operations on the input data.

Preprocessing

For our task we have explored some of the preprocessing steps including patch normalization, contrast stretching and local contrast normalization. For all the experiments, we normalize each input patch by subtracting the patch mean and dividing by the standard deviation per patch. Also, all the input patches are vectorized before being fed to the predictor.

3.2 Cluster Learning

In this model we find common local structures within the data using clustering. Image patches are clustered to find a common set of locally appearing structures within the image. As we know the ground truth annotations associated to each image patch, we find the

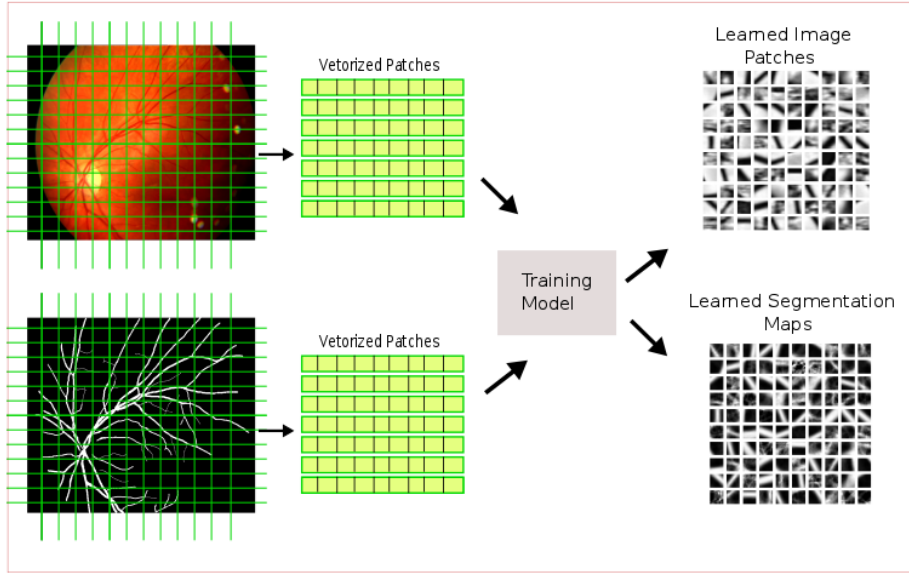


Fig. 3.2 Training architecture for our learning model.

segmentation maps for our clustered structures by associating each segmentation image patch to its corresponding cluster. In this way we learn a dictionary in the form of {image patch : segmentation} which is then used to find segmentation map for new patches. This method is inspired in part by work of Lim et al. [26] where they learn commonly occurring structures by clustering on annotated segmentation patches.

We call our method as 'Cluster Based - Common Local Structures(CB-CLS)'. Figure 3.3 shows an example of learned dictionary on drive dataset.

In the next section we describe in detail the implementation of learning and prediction steps of our algorithm.

3.2.1 Learning

The training procedure for our method requires learning clusters within the input patches. Training is performed on the patches drawn from the input images I_1, I_2, \dots, I_n and corresponding segmentation images S_1, S_2, \dots, S_n .

From the training images, we compute a random subset of m patches of fixed size $\sqrt{n} \times \sqrt{n}$ and their corresponding annotation as computed from the segmentation images. This subset of patches is used to learn a representative dictionary of patches representing the locally occurring structures in the image and the associated segmentation maps. Let us denote a patch as x_i and its corresponding segmentation map patch as y_i . Then the new training set can be represented as:

$$X = \{x_1, x_2, \dots, x_n\}$$

$$Y = \{y_1, y_2, \dots, y_n\}$$

In the next step we find 'k' clusters within the patches in X using K-Means clustering as explained in 2.2.1. Let the 'k' learned cluster be denoted as $C = \{C_1, C_2, \dots, C_k\}$ where the clusters then can be represented by their cluster centroids c_1, c_2, \dots, c_k . A cluster with 'm' patches then can be represented as

$$C_k = \{x_1^k, x_2^k, \dots, x_m^k\}$$

Now, since we know the annotation y_i for each training patch x_i , the image patches in each cluster can be replaced with their corresponding annotation patches to obtain a group of segmentation cluster where each such cluster can be represented as:

$$SC_k = \{y_1^k, y_2^k, \dots, y_m^k\}$$

We then represent each segmentation cluster by the average of all the points within that cluster, found as:

$$sc_k = \frac{1}{m} \sum_{i=1}^m y_m^k$$

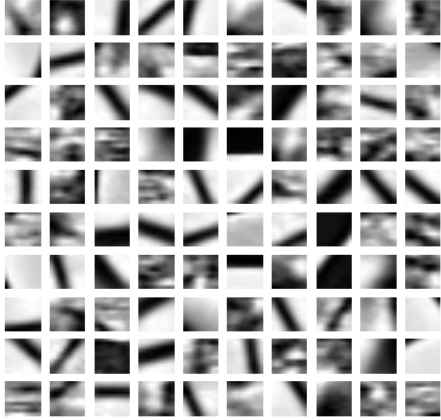
Finally, we obtain a dictionary which maps the image cluster to a ground truth segmentation patch.

$$D = \{(C_k : sc_k) | k = 1..m\}$$

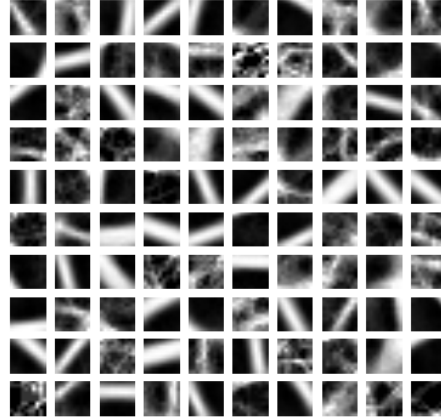
An example of a learned dictionary over image patches on DRIVE dataset is shown in Figure 3.3

3.2.2 Prediction

At test time, to predict the segmentation map for an image, we start by extracting dense patches centered at all pixel in the image. For each extracted patch its cluster membership is predicted using the already trained clustering model. The cluster labels are then matched in the dictionary to obtain the respective segmentation map for the patch. Output image is reconstructed from the patch annotations by averaging.



(a) Learned cluster centers.



(b) Segmentation maps for learned clusters.

Fig. 3.3 The image on the left shows the local structures appearing in the images. We can see a mix of straight lines at different orientations and other complex structures. The vessels are in black. The image on the right depicts the corresponding vessels. Vessel pixels are in white and the background in black.

3.2.3 Algorithm

The entire learning algorithm than can be summarized in following steps:

1. Extract a set of random Image-Segmentation patches of size $m \times m$ from the training images.
2. Train a K-Means clustering model on the input image patches and learn k clusters on the input.
3. Compute the ground truth patch for each cluster by averaging the ground truth annotations for each patch belonging to a cluster.
4. Construct a dictionary of Cluster and annotations.

3.3 Dictionary Learning

The model is based on learning an over-complete dictionary over the training data. We aim to learn a good dictionary which can represent our data as a sparse linear combination of the dictionary atoms. This method is similar to our previous method where also we learn a dictionary which represents the local structures within the data. The mathematical reasoning

behind is that, a signal (in our case an image) can be represented as a combination of a small number of basic structures, like edges and lines. It is also easy to obtain the segmentation maps for such basic atoms. In our method, for each such image patch, denoted as dictionary atoms, we find a corresponding segmentation label patch from the given segmentation map for the image.

For example, given an over complete dictionary of atoms $D \in R^{m,k}$, with k columns as the learned image atoms, we can reconstruct a given image patch $x \in R^m$ as a linear combination of atoms in D . More formally, we learn a sparse code α over D to represent x as

$$x \approx D\alpha$$

This is very similar to our cluster based method. The learned cluster centers can be considered as the dictionary with the cluster centers at dictionary atoms. And each point within a cluster can be represented as a linear combination of clusters centers with coefficients α , constrained as $\|\alpha\|_0$. This constraint forces our data point to be represented by only one cluster.

The advantage of the dictionary learning method is that it can represent complex structures like t-junctions and crossover regions much more accurately as a combination of various atoms. As the local structures are learned in dictionaries, we call our method as 'Common Local Structures in Learned Dictionaries(CL-S-LD)' In the following section we describe the implementation of the learning model.

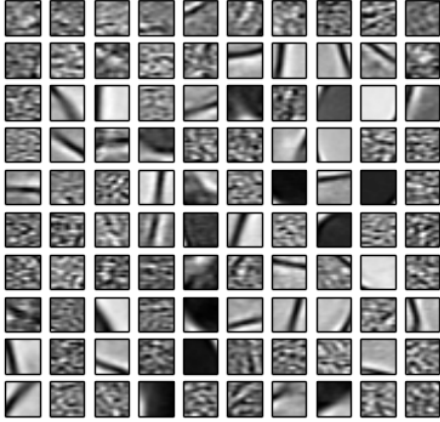
3.3.1 Learning

The learning phase starts by extracting image and label patches from the training data. Let us represent our training set composed of random patches as,

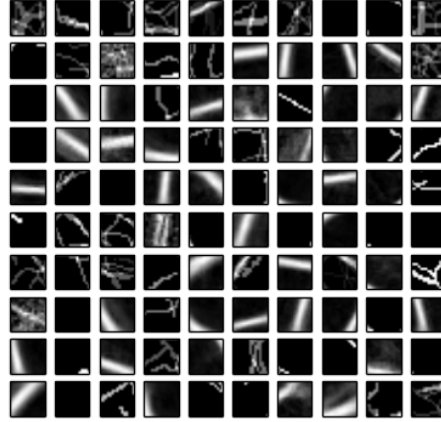
$$X = \{x_1, x_2, \dots, x_n\}$$

$$Y = \{y_1, y_2, \dots, y_n\}$$

where X is composed of image patches and Y the corresponding label patches. Each image patch can be represented as a vector by concatenating each of the pixel values. So given, 'm' patches of size $\sqrt{n} \times \sqrt{n}$, the dataset can than be represent as matrices $X, Y \in R^{m,n}$. Each row in the matrix denotes a patch or image atom.



(a) Dictionary D of atoms learned on the raw image patches



(b) Dictionary L, consisting of computed segmentation maps for atoms in D

Fig. 3.4 The image on the left shows the learned representative atoms on raw image patches. Most of the atoms depict simple structures like lines and edges. The vessels are in black. The image on the right depicts the corresponding vessels. Vessel pixels are in white and the background in black.

We learn an over complete dictionary D of basis atoms from the image patches using the dictionary learning methods as described in section 2.3. The aim is to learn a dictionary D with k atoms which can best represent x_i using linear combination of a few atoms d_k of the learned dictionary.

In the next step we learn a sparse code α to represent our input X in terms of dictionary atoms.

$$X = \alpha D$$

Since we already know the ground truth annotation Y for X, we can infer that Y can be approximately represented as a linear combination of atoms from a dictionary of labels L, corresponding to D.

As the sparse code remains same for both the representations, we can compute the dictionary atoms from L by taking a weighted average of all the ground truth patches in Y, weighed by sparse codes for all the patches.

So we learn two dictionaries, D of image patches and L consisting of label patches corresponding to atoms in D. An example of the learned dictionaries D and L over DRIVE dataset is shown in figure 3.4

3.3.2 Prediction

At the test time, given an image I , dense patches can be computed and the image can be represented as a matrix $I \in \mathbb{R}$, where each row represents a patch of size $n \times n$. We then compute a sparse decomposition of I over dictionary D represented by a sparse code α such that:

$$I = D\alpha$$

We can then compute the ground truth segmentation S , for the image patches in I , as :

$$S = L\alpha$$

where α is the sparse code computed over dictionary D and L is the label dictionary previously computed during the learning phase.

3.4 Datasets

For testing the performance of our algorithm, we train and test our system on the following publicly available datasets. In this section we describe the characteristics of these datasets

3.4.1 DRIVE

The Digital Retinal Images for Vessel Extraction (DRIVE) dataset [43] consists of 40 color retinal images randomly selected from diabetic retinopathy screening program for 400 diabetic patients. Each of these images in dataset are JPEG compressed and have a dimensions of 768 x 584 pixels captured at a resolution on bits per pixel. The images are captured with a 45degree field of view (FOV). Of the 40 images in the dataset, 7 show sign of diabetic retinopathy, while the remaining 33 do not consist of any pathology. Each image is provided with a corresponding mask delineating the FOV.

The dataset is provided with divisions in terms of training and testing set, with each set consisting of 20 images. Each of the 40 images have been manually segmented by human observers trained by an experienced ophthalmologist. For the training set, single ground truth segmentation of the vessels is provided. The test set is provided with two ground truth segmentations, of which the first one is used as gold standard and the other is used to compare the performance with an independent human observer.

3.4.2 STARE

The STARE dataset [17, 18] consists of 20 images with blood vessel segmentations, out of which 10 show signs of pathology. The images have been capture with a FOV of 35degrees at 8 bit per pixel resolution, with dimensions of each image as 605 x 700 pixels. The dataset consists of segmentation provided by two human observers. In our experiments, we consider the segmentations provided by the first observer as ground truth.

For the experiments, the dataset is randomly divided into training and test sets each consisting of 10 images.

3.4.3 ARIA

The ARIA dataset [10, 50] consists of three groups of images. One of the group consists of 92 images with age-related macular degeneration, the other with 59 images from diabetic patients and the last group with 61 images from a control group.

The images are captures with a 50degree FOV, stored in uncompressed TIFF format, with a resolution of 8bits per pixel. Each image has dimensions of 768 x 576 pixels. The dataset provides with blood vessel segmentation images as manually segmented by experts and a corresponding mask delineating the FOV region.

Table 3.1 Summary of Datasets

Datasets	FOV	# of Images
DRIVE	45	20+20
STARE	30	20
ARIA	50	212
CHASEDB1	30	28

3.4.4 CHASEDB1

The CHASEDB1 dataset [13] consist of 28 images captured at 30degree FOV with a resolution of 1280 x 960 pixels.The dataset consists of two images per patient(one for each eye) captured for 14 children.

Chapter 4

Experimental Evaluation and Results

In this chapter we present the quantitative and qualitative evaluations of our learning algorithms as described in the last chapter. All the experiments are performed on the green channel of the image as it has the maximum contrast between the vessel and background as can be seen in Fig 4.1.

The performance of the proposed vessel segmentation algorithm is evaluated using the segmented vasculature considered as the gold standard and the manually marked segmentations by the human observer. All prior work with which we compare our method, have done a segmentation performance analysis with the manual segmentations provided by the first human observer. Additionally for some of the datasets we have a manual segmentation provided by the second observer which can be used to compare the automated methods to that of manual segmentations.

To asses the performance of segmentation methods, various metric have been defined in literature [33, 40]. As reported in prior works, we also compute the performance of our vessel segmentation model defined as, true positives (TP): number of correctly classified vessel pixels; false positives (FP): number of pixels falsely classified as vessels; true negatives(TN): number of correctly classified non-vessel pixels; false negatives(FN): number of pixels falsely classified as non-vessels.

Using these metrics we can compute the accuracy (number of TP+TN / total pixels), pixel classification sensitivity and specificity. We also calculate the area under curve for receiver operation characteristics and the precision recall curve obtained by varying the threshold value for the segmented images.

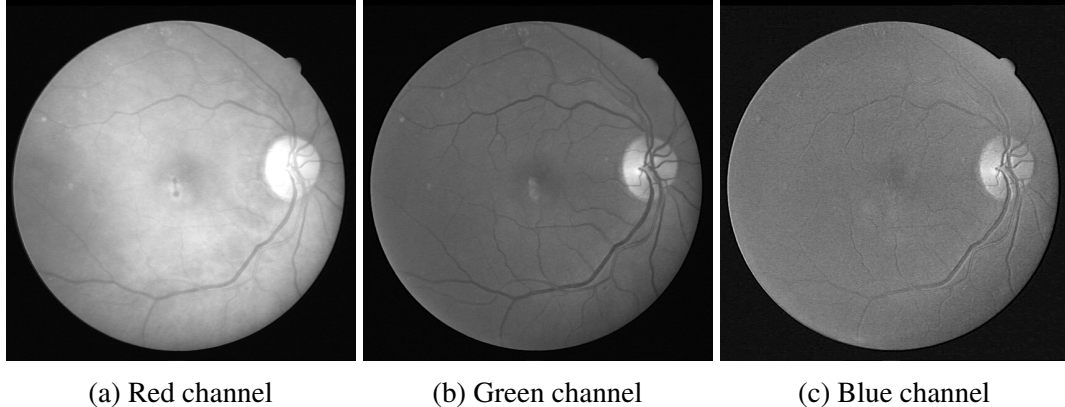


Fig. 4.1 Different channels of a fundus image showing variation in contrast of blood vessels against background. Green channel shows the maximum contrast in blood vessels and background.

For a complete assessment of our segmentation model, we perform various experiments. We start by performing the experiment on all the 4 datasets and compute the performance metrics as described above. Next, to test the generalization of our system we do cross training, i.e, training on images from one dataset and prediction on other. We test the performance of both our models.

4.1 Vessel Segmentation Assessment

The proposed models have some input parameters, which need to be evaluated to have the best performance on the models. We start by exploring the various parameters and discuss their effect on our model.

One of the main parameters of our model is the patch size. As this is a patch based framework the size of patch is very important to us. A small patch size would mean that we may not be able to extract sufficient local information and a bigger patch size would mean that the local structure information would be lost as the patch may constitute multiple local structures. Also as we perform an averaging based reconstruction, the pixel value might get reduced to a very small value during reconstruction due to presence of lot of background pixels.

We test our model on a multitude of patch size varying from (10,10) to (21,21). The segmentation results for various patch size on an image are show in 4.2. From the segmentation results, we infer that as the patch size is slowly increased we lose out on the finer details. A

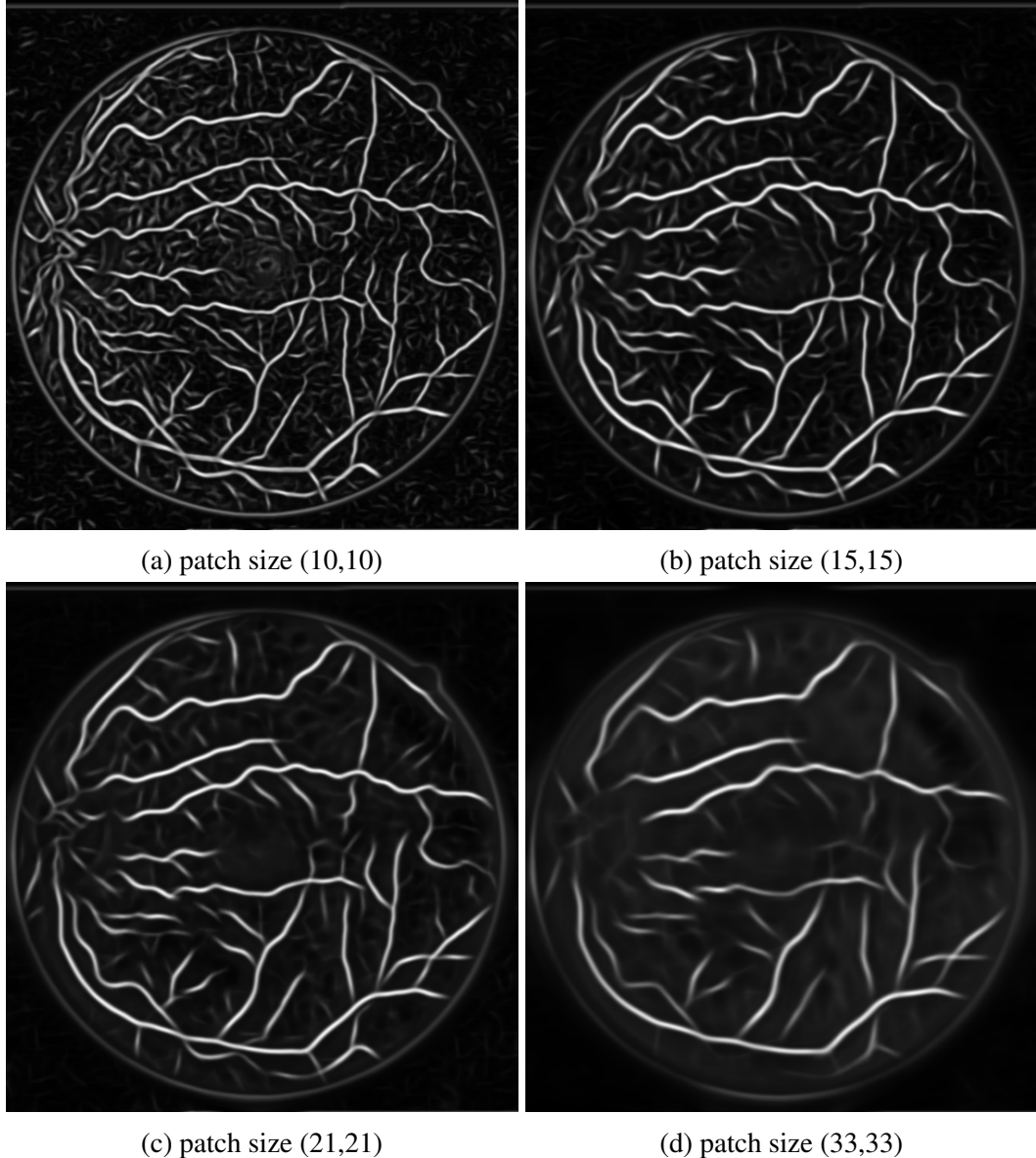
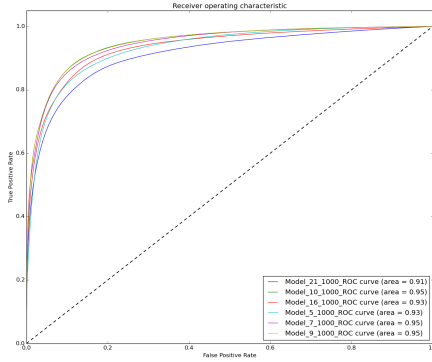


Fig. 4.2 Here we show the effect of varying patch size in our patch based framework. As we increase the patch size, we lose details on thin vessels, but our confidence on thick vessels increases.



(a) ROC curve

Fig. 4.3 ROC curve, comparing the performance of our model on DRIVE test set with varying patch sizes.

larger patch size is able to segment out thick vessels but doesn't perform well on thin vessels. Visually examining the results, patch size of (10,10) and (15,15) give satisfactory results. Figure 4.3 shows the ROC curve for DRIVE test set with varying patch size applied with a cluster size K of 1000.

The next important parameter in our model is 'K' the number of clusters. The number of clusters forms an important factor in both our models. It determines, the number of local structures we wish to learn from the dataset. Too small a number and we would miss some important local structures present in our data. Increasing the number of clusters beyond a point doesn't add any benefit, but might increase the time complexity. In the dictionary learning model, the number of clusters in general should be larger than the dimension of our feature vectors, to learn an overcomplete dictionary. As we can see in figure 4.4, a small number of cluster size leads to a lot of noise due to mismatched ground truth annotations.

No we evaluate the segmentation performance of our Cluster Based Common Local Structure classifier (CB-CLS), by training it on the DRIVE train and testing on DRIVE test dataset. The train parameters are set as , patch size of (10,10) with number of clusters K=1000. The Precision recall curve and receiver operation characteristics for our solution is shown in figure 4.5

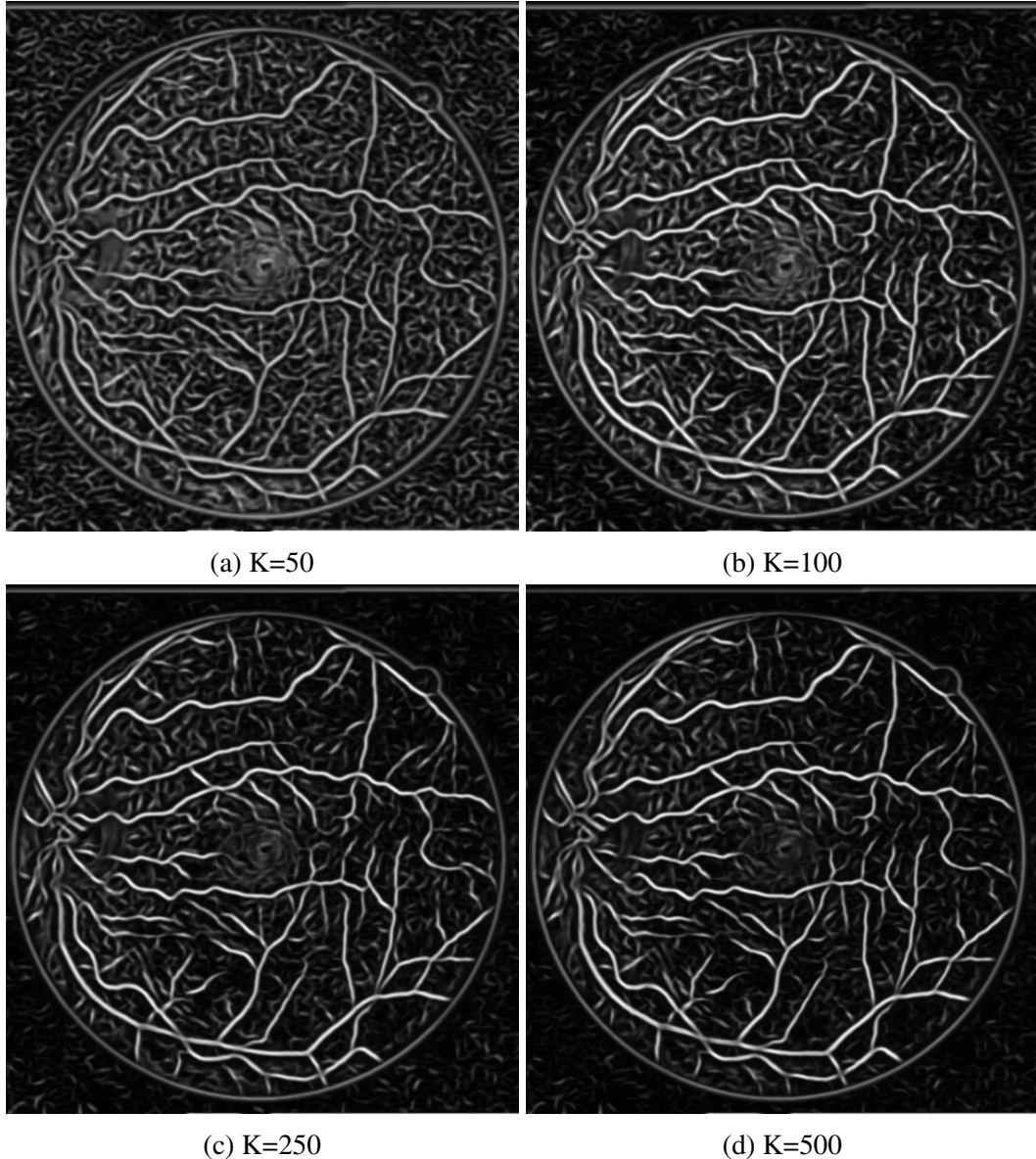


Fig. 4.4 Here we show the effect of varying the number of clusters in our patch based framework.

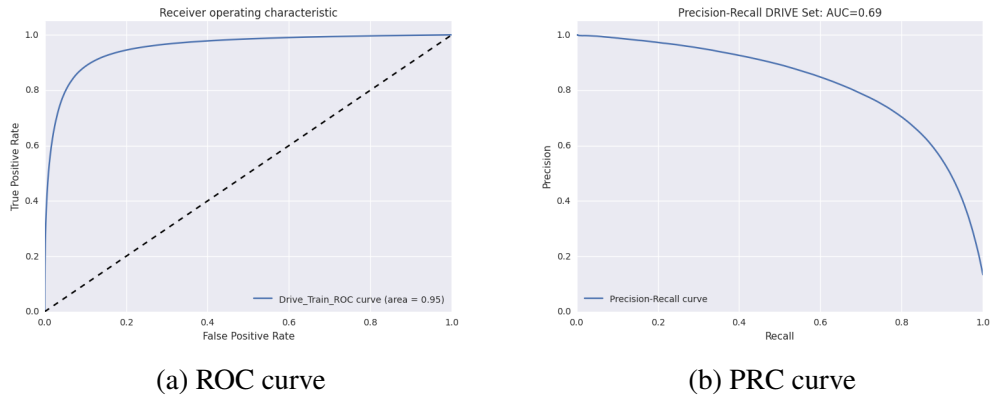
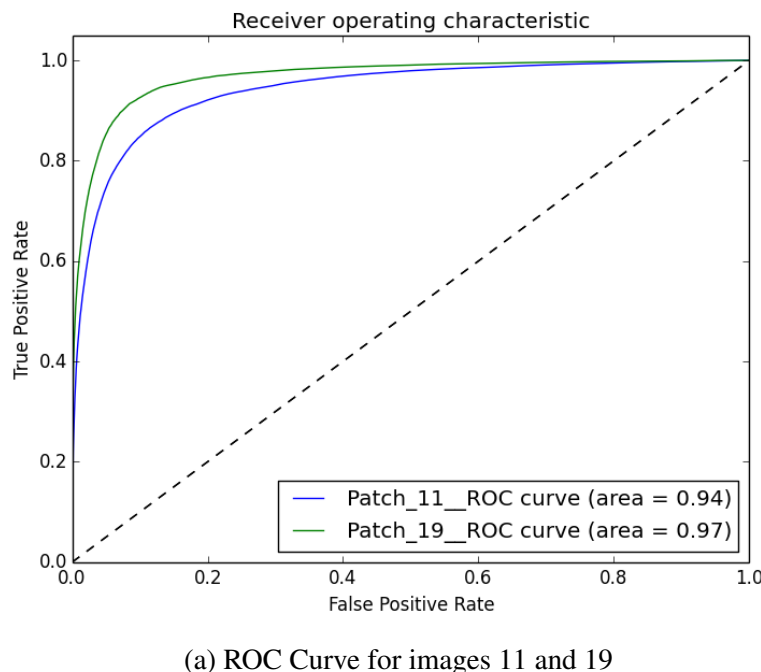


Fig. 4.5 Receiver operation characteristics curve and precision recall curve showing the performance of the Cluster Learning model, compared to ground truth annotation.



(a) ROC Curve for images 11 and 19

Fig. 4.6 ROC curve comparing the best and worse case images on DRIVE dataset.

Table 4.1 STARE performance for different training sets

Datasets	AUC
DRIVE Train	0.949
STARE	0.957 (Training AUC)
ARIA	0.945
CHASEDB1	0.943

A comparison of our model with other methods in literature is shown in figure 4.7.

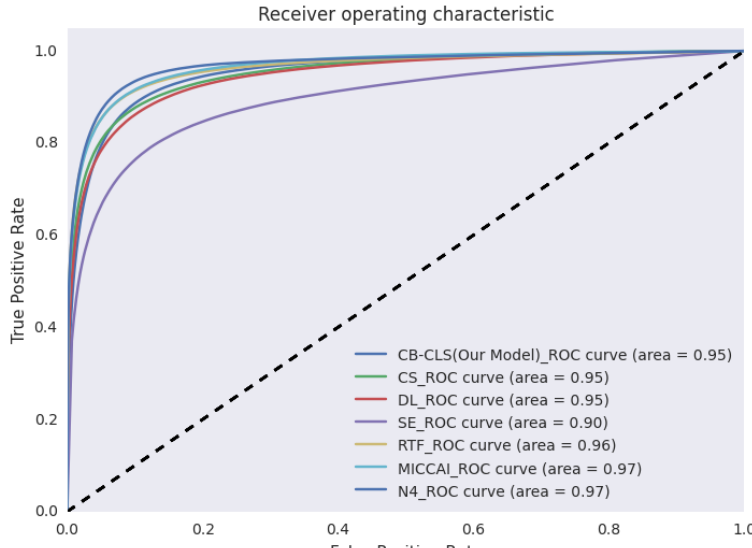
As we can see, that our cluster learning model has a decent performance and performs better than the structure forests model(SE) proposed by Dollár and Zitnick [8]. Also it has a comparable performance to the dictionary learning(DL) based model proposed by Rigamonti et al. [39] and the linear filter model(CS) proposed by Rigamonti and Lepetit [38].

We then compare the best case and worst case in our model. For the best case the AUC is 0.97 and for the worst case the AUC is 0.94. The best case and worst case segmentations are shown in figure 4.9 and figure 4.10 respectively. Note that the images are not thresholded. The threshold for false positive rate (FPR) of 0.05 is 0.72 as shown in figure 4.6. We observe that for the best case scenario, the segmentation is better near the optic nerve. In the worst case scenario, we get a very poor segmentation near the optic nerve region.

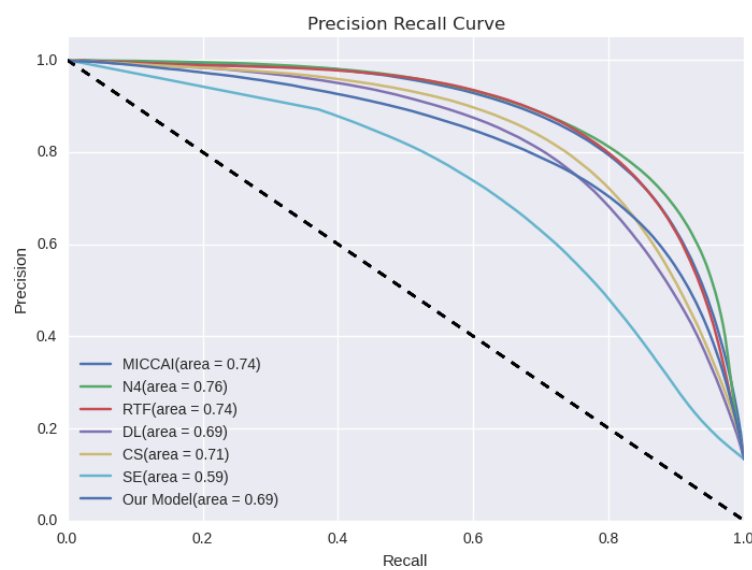
We also compare our model on the stare dataset. As there is no division of dataset provided, to asses the performance of our algorithm we randomly divide the dataset into training and test set with equal number of images. For the stare set we obtain a decent performance with an AUC of 0.96 as shown in figure 4.8

4.2 Generalization of the model

To check if our model is dependent on the training dataset, we perform an experiment by cross training. We train our model with DRIVE dataset, ARIA dataset and CHASEDB dataset, and compute our predictions on the full STARE dataset. The AUC curves for all the three trainings are shown in figure 4.11. We observe that the performance on the STARE dataset is similar for all the underlying training procedures using different datasets. This shows the generalization capabilities of our model. The AUC results for the different training are shown in the table 4.1

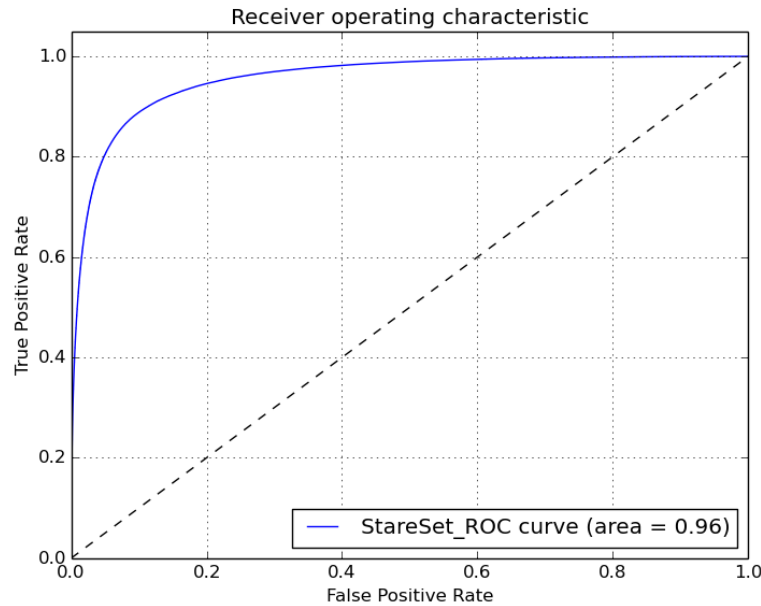


(a) ROC Curve



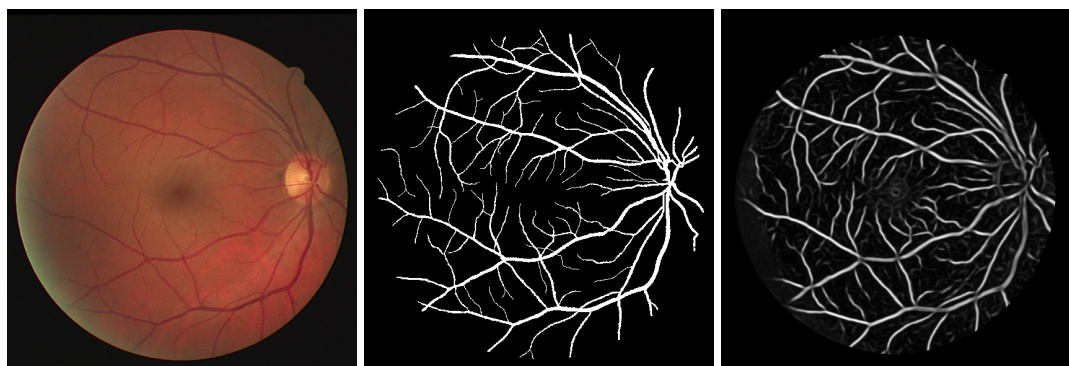
(b) PRC Curve

Fig. 4.7 We compare our model by testing it on the DRIVE dataset. Results are shown for some of the state-of-art methods in literature. SE is the structured forest model by Dollár and Zitnick [8], DL is the dictionary leaned filter model by Rigamonti et al. [39], CS is the linear filter model by Rigamonti and Lepetit [38], N4 is the CNN-kNN model by Ganin and Lempitsky [15], MICCAI is the method proposed by Becker et al. [2]



(a) ROC Curve

Fig. 4.8 ROC curve for the STARE dataset.

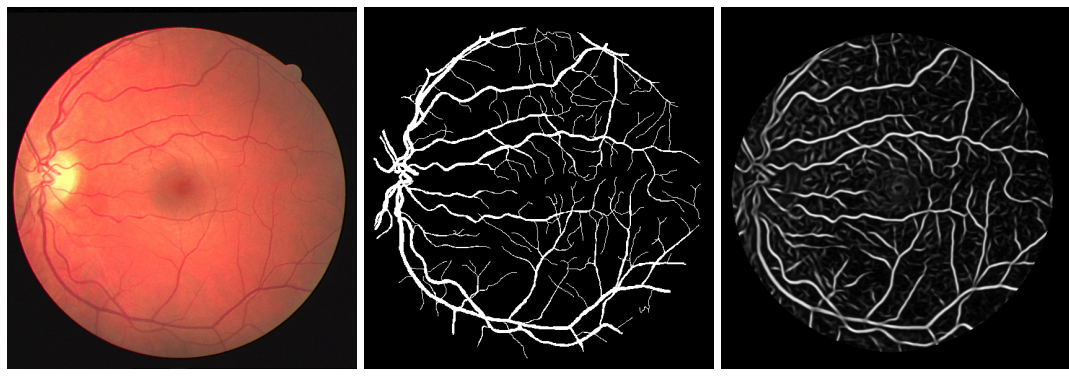


(a) Original image

(b) Ground truth segmentation

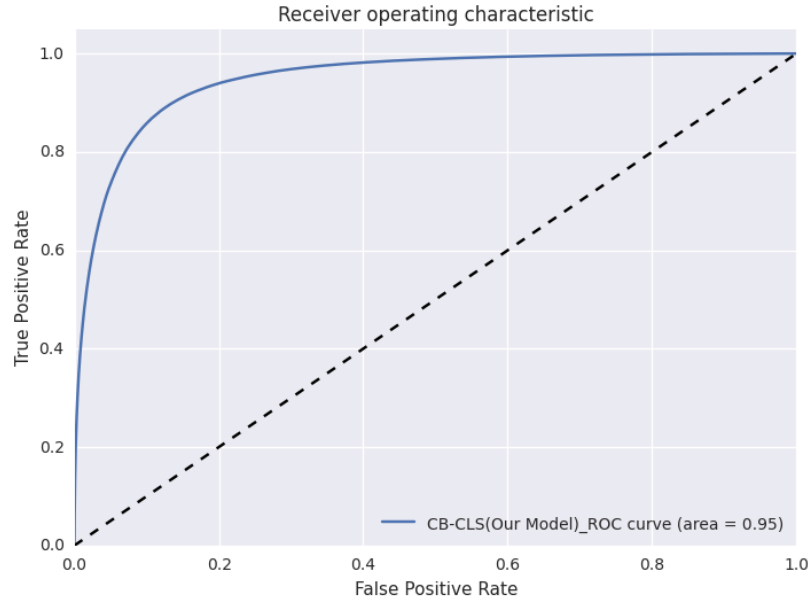
(c) Proposed segmentation

Fig. 4.9 This is the best case on DRIVE test dataset, when predicted using the CB-CLS model. The AUC for the proposed solution is 0.97

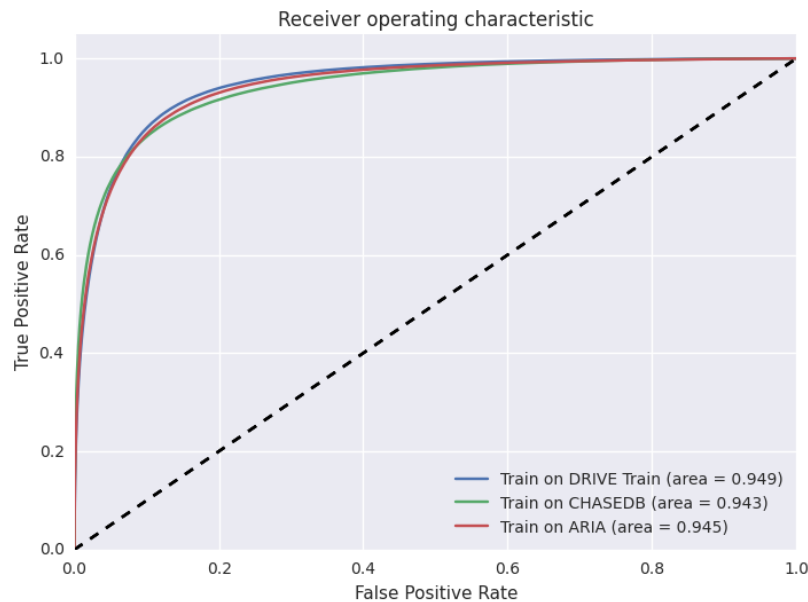


(a) Original image (b) Ground truth segmentation (c) Proposed segmentation

Fig. 4.10 This is the worst case on DRIVE test dataset, when predicted using the CB-CLS model. The AUC for the proposed solution is 0.94



(a) ROC of STARE trained on DRIVE



(b) ROC for STARE

Fig. 4.11 We train our classifier on DRIVE, ARIA and CHASEDB dataset and the predictions are made on STARE set. The ROC curves for all the predictions are shown

Chapter 5

Conclusion and Future Work

In this study, we proposed two new learning approaches to solve the problem of vessel segmentation in fundus images. Our models are based on a learning framework from training data. Our models exploit the presence of frequently occurring basic structures in retinal vessels. In our models, we characterize the presence of structures like edges and straight lines. The model named Cluster Based - Common local structures (CB-CLS), is a partially supervised learning method. We start by learning the common patterns within the raw data by an unsupervised clustering approach and then assigning segmentation maps to them from given segmentation maps.

The model works well in predicting thick vessels and parallel vessels. The second model is basically an extension of the first model, where we learn the structures and annotations in a sparse coding dictionary learning framework. Our model, Common Local Structures in Learned dictionaries (CLS-LD), represent each individual patch as a sparse linear combination of dictionary atoms. This helps us to approximate t-junctions and bifurcations in a better way. The preliminary results for our Dictionary learning model were similar to that of the other model. The models requires further tuning and some experiments to verify the capabilities of it. Our methods though very simple, demonstrated good performance compared to the current state-of-art methods.

One of the key contribution in the thesis is a generalizable vessel segmentation model, which is partially independent to the training dataset. Our model has very little dependence on the training data as compared to some other methods whose performance depend on the underlying training data. This comes from the fact that the model exploits the presence of common structures and utilizes them to make structured segmentation prediction at patch level.

Our model though not optimized with speed in mind, has a reasonably fast run time of approximately 4sec per image for an image size of 584 x 565 pixels. This is the total

prediction time per image. With code optimization we can further reduce the run time of our mode. At present we are predicting the patches at all the pixels. By using some initial preprocessing methods, we can get an average segmentation and predict on only the relevant pixels thereby further reducing the run time.

The future work would be aimed at extending these methods. Some of the following things we should look into:

- Our models do not segment out the very thin vessels perfectly. We should look into extending the model in a way to extract thin vessels. As most of the methods do work very well on the thick vessels, one way to look into it is to have separate models for thin and thick vessels.
- The dictionary learning model needs more evaluation. We believe that with better tuning and learning better dictionaries we would be able to estimate the segmentation at crossover regions and bifurcation zones much reliably.
- At present we make a dense prediction i.e, we make predictions on all the pixel including the obvious background pixels. By using preprocessing methods or utilizing basic edge detectors, we can detect the points of interest and make prediction much more efficiently.
- We should validate our model on other similar problems of vessel segmentation in medical images.

References

- [1] Al-Rawi, M., Qutaishat, M., and Arrar, M. (2007). An improved matched filter for blood vessel detection of digital retinal images. *Computers in Biology and Medicine*, 37(2):262–267.
- [2] Becker, C., Rigamonti, R., Lepetit, V., and Fua, P. (2013). Supervised feature learning for curvilinear structure segmentation. In *Medical Image Computing and Computer-Assisted Intervention—MICCAI 2013*, pages 526–533. Springer.
- [3] Calvo, D., Ortega, M., Penedo, M. G., and Rouco, J. (2011). Automatic detection and characterisation of retinal vessel tree bifurcations and crossovers in eye fundus images. *Computer methods and programs in biomedicine*, 103(1):28–38.
- [4] Chrástek, R., Wolf, M., Donath, K., Michelson, G., and Niemann, H. (2002). Optic disc segmentation in retinal images. In *Bildverarbeitung für die Medizin 2002*, pages 263–266. Springer.
- [5] Chutatape, O., Zheng, L., and Krishnan, S. (1998a). Retinal blood vessel detection and tracking by matched gaussian and kalman filters. In *Engineering in Medicine and Biology Society, 1998. Proceedings of the 20th Annual International Conference of the IEEE*, volume 6, pages 3144–3149. IEEE.
- [6] Chutatape, O., Zheng, L., and Krishnan, S. (1998b). Retinal blood vessel detection and tracking by matched gaussian and kalman filters. In *Engineering in Medicine and Biology Society, 1998. Proceedings of the 20th Annual International Conference of the IEEE*, volume 6, pages 3144–3149. IEEE.
- [7] Doi, K. (2007). Computer-aided diagnosis in medical imaging: historical review, current status and future potential. *Computerized medical imaging and graphics*, 31(4):198–211.
- [8] Dollár, P. and Zitnick, C. L. (2013). Structured forests for fast edge detection. In *Computer Vision (ICCV), 2013 IEEE International Conference on*, pages 1841–1848. IEEE.
- [9] Donoho, D. L. (2006). Compressed sensing. *Information Theory, IEEE Transactions on*, 52(4):1289–1306.
- [10] Farnell, D. J., Hatfield, F., Knox, P., Reakes, M., Spencer, S., Parry, D., and Harding, S. (2008). Enhancement of blood vessels in digital fundus photographs via the application of multiscale line operators. *Journal of the Franklin institute*, 345(7):748–765.

- [11] Frangi, A. F., Niessen, W. J., Vincken, K. L., and Viergever, M. A. (1998). Multiscale vessel enhancement filtering. In *Medical Image Computing and Computer-Assisted Intervention—MICCAI'98*, pages 130–137. Springer.
- [12] Fraz, M. M., Remagnino, P., Hoppe, A., Uyyanonvara, B., Rudnicka, A. R., Owen, C. G., and Barman, S. A. (2012a). Blood vessel segmentation methodologies in retinal images—a survey. *Computer methods and programs in biomedicine*, 108(1):407–433.
- [13] Fraz, M. M., Remagnino, P., Hoppe, A., Uyyanonvara, B., Rudnicka, A. R., Owen, C. G., and Barman, S. A. (2012b). An ensemble classification-based approach applied to retinal blood vessel segmentation. *Biomedical Engineering, IEEE Transactions on*, 59(9):2538–2548.
- [14] Fuller, A. R., Zawadzki, R. J., Choi, S., Wiley, D. F., Werner, J. S., and Hamann, B. (2007). Segmentation of three-dimensional retinal image data. *Visualization and Computer Graphics, IEEE Transactions on*, 13(6):1719–1726.
- [15] Ganin, Y. and Lempitsky, V. (2014). N4-fields: Neural network nearest neighbor fields for image transforms. *arXiv preprint arXiv:1406.6558*.
- [16] Gardner, G., Keating, D., Williamson, T., and Elliott, A. (1996). Automatic detection of diabetic retinopathy using an artificial neural network: a screening tool. *British journal of Ophthalmology*, 80(11):940–944.
- [17] Hoover, A. and Goldbaum, M. (2003). Locating the optic nerve in a retinal image using the fuzzy convergence of the blood vessels. *Medical Imaging, IEEE Transactions on*, 22(8):951–958.
- [18] Hoover, A., Kouznetsova, V., and Goldbaum, M. (2000). Locating blood vessels in retinal images by piecewise threshold probing of a matched filter response. *Medical Imaging, IEEE Transactions on*, 19(3):203–210.
- [19] Huang, K. and Aviyente, S. (2006). Sparse representation for signal classification. In *Advances in neural information processing systems*, pages 609–616.
- [20] Jiang, X. and Mojon, D. (2003). Adaptive local thresholding by verification-based multithreshold probing with application to vessel detection in retinal images. *Pattern Analysis and Machine Intelligence, IEEE Transactions on*, 25(1):131–137.
- [21] Kanungo, T., Mount, D. M., Netanyahu, N. S., Piatko, C. D., Silverman, R., and Wu, A. Y. (2002). An efficient k-means clustering algorithm: Analysis and implementation. *Pattern Analysis and Machine Intelligence, IEEE Transactions on*, 24(7):881–892.
- [22] Law, M. W. and Chung, A. C. (2008). Three dimensional curvilinear structure detection using optimally oriented flux. In *Computer Vision—ECCV 2008*, pages 368–382. Springer.
- [23] Leandro, J. J., Cesar, R. M., and Jelinek, H. F. (2001). Blood vessels segmentation in retina: Preliminary assessment of the mathematical morphology and of the wavelet transform techniques. In *Computer Graphics and Image Processing, 2001 Proceedings of XIV Brazilian Symposium on*, pages 84–90. IEEE.

- [24] Lee, H., Battle, A., Raina, R., and Ng, A. Y. (2006). Efficient sparse coding algorithms. In *Advances in neural information processing systems*, pages 801–808.
- [25] Lewicki, M. and Sejnowski, T. (2000). Learning overcomplete representations. *Neural computation*, 12(2):337–365.
- [26] Lim, J. J., Zitnick, C. L., and Dollár, P. (2013). Sketch tokens: A learned mid-level representation for contour and object detection. In *Computer Vision and Pattern Recognition (CVPR), 2013 IEEE Conference on*, pages 3158–3165. IEEE.
- [27] MacQueen, J. et al. (1967). Some methods for classification and analysis of multivariate observations. In *Proceedings of the fifth Berkeley symposium on mathematical statistics and probability*, volume 1, pages 281–297. Oakland, CA, USA.
- [28] Mairal, J., Bach, F., Ponce, J., and Sapiro, G. (2009a). Online dictionary learning for sparse coding. In *Proceedings of the 26th Annual International Conference on Machine Learning*, pages 689–696. ACM.
- [29] Mairal, J., Bach, F., Ponce, J., and Sapiro, G. (2010). Online learning for matrix factorization and sparse coding. *The Journal of Machine Learning Research*, 11:19–60.
- [30] Mairal, J., Ponce, J., Sapiro, G., Zisserman, A., and Bach, F. R. (2009b). Supervised dictionary learning. In *Advances in neural information processing systems*, pages 1033–1040.
- [31] Mendonca, A. M. and Campilho, A. (2006). Segmentation of retinal blood vessels by combining the detection of centerlines and morphological reconstruction. *Medical Imaging, IEEE Transactions on*, 25(9):1200–1213.
- [32] Mnih, V. and Hinton, G. E. (2012). Learning to label aerial images from noisy data. In *Proceedings of the 29th International Conference on Machine Learning (ICML-12)*, pages 567–574.
- [33] Monteiro, F. C. and Campilho, A. C. (2006). Performance evaluation of image segmentation. In *Image Analysis and Recognition*, pages 248–259. Springer.
- [34] Nguyen, U. T., Bhuiyan, A., Ramamohanarao, K., and Park, L. A. (2011). An effective supervised framework for retinal blood vessel segmentation using local standardisation and bagging. In *Machine Learning in Medical Imaging*, pages 117–125. Springer.
- [35] Niemeijer, M., van Ginneken, B., Russell, S. R., Suttorp-Schulten, M. S., and Abramoff, M. D. (2007). Automated detection and differentiation of drusen, exudates, and cotton-wool spots in digital color fundus photographs for diabetic retinopathy diagnosis. *Investigative ophthalmology & visual science*, 48(5):2260–2267.
- [36] Pati, Y. C., Rezaifar, R., and Krishnaprasad, P. (1993). Orthogonal matching pursuit: Recursive function approximation with applications to wavelet decomposition. In *Signals, Systems and Computers, 1993. 1993 Conference Record of The Twenty-Seventh Asilomar Conference on*, pages 40–44. IEEE.

- [37] Ricci, E. and Perfetti, R. (2007). Retinal blood vessel segmentation using line operators and support vector classification. *Medical Imaging, IEEE Transactions on*, 26(10):1357–1365.
- [38] Rigamonti, R. and Lepetit, V. (2012). Accurate and efficient linear structure segmentation by leveraging ad hoc features with learned filters. In *Medical Image Computing and Computer-Assisted Intervention–MICCAI 2012*, pages 189–197. Springer.
- [39] Rigamonti, R., Sironi, A., Lepetit, V., and Fua, P. (2013). Learning separable filters. In *Computer Vision and Pattern Recognition (CVPR), 2013 IEEE Conference on*, pages 2754–2761. IEEE.
- [40] Sharma, M. (2001). Performance evaluation of image segmentation and texture extraction methods in scene analysis.
- [41] Sopharak, A., Dailey, M. N., Uyyanonvara, B., Barman, S., Williamson, T., Nwe, K. T., and Moe, Y. A. (2010). Machine learning approach to automatic exudate detection in retinal images from diabetic patients. *Journal of Modern optics*, 57(2):124–135.
- [42] Staal, J., Abràmoff, M. D., Niemeijer, M., Viergever, M. A., and van Ginneken, B. (2004a). Ridge-based vessel segmentation in color images of the retina. *Medical Imaging, IEEE Transactions on*, 23(4):501–509.
- [43] Staal, J., Abràmoff, M. D., Niemeijer, M., Viergever, M. A., and van Ginneken, B. (2004b). Ridge-based vessel segmentation in color images of the retina. *Medical Imaging, IEEE Transactions on*, 23(4):501–509.
- [44] Tolias, Y. A. and Panas, S. M. (1998). A fuzzy vessel tracking algorithm for retinal images based on fuzzy clustering. *Medical Imaging, IEEE Transactions on*, 17(2):263–273.
- [45] Tropp, J. A. and Gilbert, A. C. (2007). Signal recovery from random measurements via orthogonal matching pursuit. *Information Theory, IEEE Transactions on*, 53(12):4655–4666.
- [46] Vega, R., Guevara, E., Falcon, L. E., Sanchez-Ante, G., and Sossa, H. (2013). Blood vessel segmentation in retinal images using lattice neural networks. In *Advances in Artificial Intelligence and Its Applications*, pages 532–544. Springer.
- [47] Vlachos, M. and Dermatas, E. (2010). Multi-scale retinal vessel segmentation using line tracking. *Computerized Medical Imaging and Graphics*, 34(3):213–227.
- [48] Walter, T. and Klein, J.-C. (2001). Segmentation of color fundus images of the human retina: Detection of the optic disc and the vascular tree using morphological techniques. In *Medical Data Analysis*, pages 282–287. Springer.
- [49] Zana, F. and Klein, J.-C. (2001). Segmentation of vessel-like patterns using mathematical morphology and curvature evaluation. *Image Processing, IEEE Transactions on*, 10(7):1010–1019.
- [50] Zheng, Y., Hijazi, M. H. A., and Coenen, F. (2012). Automated “disease/no disease” grading of age-related macular degeneration by an image mining approach. *Investigative ophthalmology & visual science*, 53(13):8310–8318.